PLOS ONE

Crystal Structure of the Fibre Head Domain of the Atadenovirus Snake Adenovirus 1

Abhimanyu K. Singh[1,2], Rosa Menéndez-Conejero[1,2], Carmen San Martín[1,2], Mark J. van Raaij[1,2]*

1. Departamento de Estructura de Macromoleculas, Centro Nacional de Biotecnologia (CNB-CSIC), Madrid, Spain, **2.** NanoBiomedicine Initiative, Centro Nacional de Biotecnologia (CNB-CSIC), Madrid, Spain

*mjvanraaij@cnb.csic.es

Abstract

Adenoviruses are non-enveloped icosahedral viruses with trimeric fibre proteins protruding from their vertices. There are five known genera, from which only Mastadenoviruses have been widely studied. Apart from studying adenovirus as a biological model system and with a view to prevent or combat viral infection, there is a major interest in using adenovirus for vaccination, cancer therapy and gene therapy purposes. Adenoviruses from the Atadenovirus genus have been isolated from squamate reptile hosts, ruminants and birds and have a characteristic gene organization and capsid morphology. The carboxy-terminal virus-distal fibre head domains are likely responsible for primary receptor recognition. We determined the high-resolution crystal structure of the Snake Adenovirus 1 (SnAdV-1) fibre head using the multi-wavelength anomalous dispersion (MAD) method. Despite the absence of significant sequence homology, this Atadenovirus fibre head has the same beta-sandwich propeller topology as other adenovirus fibre heads. However, it is about half the size, mainly due to much shorter loops connecting the beta-strands. The detailed structure of the SnAdV-1 fibre head and other animal adenovirus fibre heads, together with the future identification of their natural receptors, may lead to the development of new strategies to target adenovirus vectors to cells of interest.

Introduction

Adenoviruses can cause respiratory disease, eye disease, myocarditis and gastro-enteritic disease (among others) and have been studied as a molecular biology model system [1], for instance mRNA splicing was first observed in adenovirus-infected cells. Adenoviruses are icosahedral, non-enveloped particles [2]. Each

icosahedral facet is formed by twelve hexon trimers [3], while a pentameric penton base sits at each of the vertices [4]. Trimeric fibre proteins protrude from each of the twelve vertices. These fibre proteins have an amino-terminal virus-binding sequence, a central shaft domain [5], and a globular, carboxy-terminal fibre head domain [6, 7] involved in initial receptor-binding. Depending on the adenovirus species, the fibre head may recognize one or more cell surface receptors such as the coxsackievirus and adenovirus receptor (CAR) [8, 9, 10], sialic acid [11], CD46/80/86 [12, 13] and desmoglein 2 [14]. This initial interaction is then followed by the penton base binding to cell surface integrins, leading to viral internalization via endocytosis [15].

The *Adenoviridae* family contains five genera: Mastadenovirus (all hitherto discovered human adenovirus types and most mammalian adenoviruses are Mastadenoviruses), Aviadenovirus (two-fibred adenoviruses exclusive to birds [16]) and the newly identified genera Atadenovirus, Siadenovirus and Ichtadenovirus [17]. Although structures of fibre proteins from canine Mastadenovirus 2 [18, 19] and a fowl Aviadenovirus [20, 21] have been determined, the fibres from Atadenoviruses, Siadenoviruses and Ichtadenoviruses are neither structurally nor functionally characterized.

Apart from the interest in adenovirus as disease-causing agents and for vaccination purposes, adenoviruses are also used as a framework for developing vectors to be used in gene and cancer therapy, thanks to their distinctive features such as a high potential trans-gene capacity, possibility of recombinant growth up to high titre, and efficient transduction [22, 23]. A potential downside of using vector systems based on human adenoviruses is that patients may have pre-established immunity against them. Use of distantly related non-human adenoviruses might be advantageous, as they may be less immunogenic and may have novel receptor-binding properties [24]. Recently we reported electron microscopy studies on Lizard Atadenovirus 2 [25] and crystallization of the fibre heads of Snake Atadenovirus 1 [26] and Turkey Siadenovirus 3 [27].

Snake Atadenovirus 1 (SnAdV-1) was first isolated from a corn snake (*Elaphe guttata*) with clinical signs of pneumonia [28] and classified as an Atadenovirus based on its sequence (GenBank entry DQ1064141.1; [29]). Like most structural proteins, the gene coding for the fibre protein is preserved in SnAdV-1, although we previously showed it encodes a 345 amino acid protein, rather than 415 as reported [26]. Sequence analysis suggested residues 234–345 may form a virus-distal, globular, carboxy-terminal head domain [26]. However, the putative SnAdV-1 fibre head domain has a very low sequence similarity with adenovirus fibre heads of known structure (between 12 and 18% sequence identity according to the EMBOSS STRETCHER program [30]). The Ovine Atadenovirus (OvAd-D) fibre head is also significantly smaller than other adenovirus fibre heads, as shown by electron microscopy [31].

In this work, we present the structure of the SnAdV-1 fibre head domain solved by X-ray crystallography, using the multi-wavelength anomalous dispersion (MAD) method. This is the first Atadenovirus for which the structure of the fibre head has been determined. Knowledge of the structure will lead to better

understanding of the infection mechanism of the virus and may allow the design of chimeric adenoviruses with novel cell targeting properties.

Materials and Methods

Expression of N-terminally six-histidine tagged SnAdV-1 fibre protein constructs 171–345 and 234–345 in *Escherichia coli*, purification by nickel affinity chromatography followed by strong anion exchange chromatography and crystallization by sitting drop vapour diffusion have been reported before [26]. Native crystallographic data were collected from three different crystals containing residues 234–345 (two different $P2_12_12_1$ space group crystal forms and one $I2_13$ space group crystal form) and, later, from one crystal containing amino acids 171–345 (*F*23 space group crystal form). As the native protein did not contain methionine residues in the 234–345 stretch, leucines 322 and 324 were mutated to methionine for selenomethionine derivatization [26]. *De novo* structure solution by MAD (multi-wavelength anomalous dispersion) was performed using a multi-wavelength dataset obtained for selenomethionine-containing crystals of the $I2_13$ space group from 234–345 construct. The AUTOSHARP pipeline [32] was used for structure solution, incorporating SHELX [33] for location of heavy atom sites, SOLOMON [34] for solvent correction and ARP-WARP [35] for density interpretation and automated model building. Eight selenium sites were found, compatible with four monomers per asymmetric unit and each monomer containing two selenomethionines, as expected (for phasing statistics, see Table 1). Model completion was done with COOT [36] and the structure refined against both the native and selenomethionine data with REFMAC [37], selecting the same reflections from both datasets for calculation of Rfree [38]. The final structures had good geometric parameters and could be refined to low R-factors (Table 1). In the structures where non-crystallographic symmetry (NCS) was present, reflections for calculation of Rfree were selected in thin shells (SFTOOLS, CCP4 [39]).

The structures of $P2_12_12_1$ crystal forms and *F*23 crystal form were solved by molecular replacement using PHASER [40] and refined. All refined crystal-lographic models were validated with MOLPROBITY [41]. The two different crystal forms belonging to the orthorhombic space group $P2_12_12_1$ both had four trimers in the asymmetric unit. The purified 171–345 construct protein crystallized in space group *F*23 after a period of about one year and density for residues 171–231 was absent, indicating a possible proteolysis event during crystallization. Refinement statistics for all models are given in Table 1. Coordinate files and structure factors will be available from the PDB under codes 4C0U ($I2_13$ selenomethionine derivative), 4D1F (first $P2_12_12_1$ crystal form), 4D1G (second $P2_12_12_1$ crystal form), 4D0V ($I2_13$ native) and 4UMI (*F*23 crystal form). Structure superpositions were performed using the secondary structure element matching option of CCP4MG [42]. Structure figures were prepared with PyMOL (The PyMOL Molecular Graphics System, Version 1.5.0.4. Schrödinger, LLC).

Table 1. Crystallographic structure solution and refinement (1 Å=0.1 nm).

Phasing	Remote	Peak	Inflection point	Overall	
Wavelength	0.9768	0.9791	0.9793		
Resolution range used (Å)	29.3–1.6	29.3–1.9	29.3–1.9		
Reflections (acentric/centric)	69500/2391	41317/2402	41283/2374		
Heavy atom sites				8 Se	
Correlation coefficient (all/weak)				60.91/52.64	
Patterson figure of merit				16.56	
Correlation coefficient (E)				0.560	
R-cullis isomorphous (acentric/centric)	0.646/0.616	0.686/0.665	−/−		
R-cullis anomalous (acentric)	0.641	0.455	0.518		
Phasing power isomorphous (acentric/centric)	1.378/0.886	0.864/0.466	−/−		
Phasing power anomalous (acentric)	1.899	2.665	2.356		
FOM[a] (acentric/centric)				0.554/0.357	
Solvent flattening[b]					
R-factor (before/after)				0.3720/0.1560	
Correlation on $|E|^2$ (before/after)				0.5492/0.9063	
Correlation on $|E|^2$/contrast (original/inverted)				0.1248/1.2247	
Refinement					
	Selenomethionine	Native 1	Native 2	Native 3	Native 4
Space group	$I2_13$	$P2_12_12_1$	$P2_12_12_1$	$I2_13$	$F23$
Cell parameters (a, b, c, Å)	149.5, 149.5, 149.5	79.6, 122.3, 133.7	96.8, 96.8, 153.3	149.6, 149.6, 149.6	121.5, 121.5, 121.5
Monomers/ asymmetric unit	4	12	12	4	1
Resolution (Å)	29.3–1.6 (1.70–1.60)[c]	29.9–2.7 (2.86–2.70)	29.7–1.9 (2.03–1.90)	29.3–1.7 (1.80–1.70)	43.0–1.33 (1.37–1.33)
Reflections used	70937 (11269)	32882 (5194)	111478 (19922)	59326 (9523)	32152 (2285)
Reflections used for R_{free}	1975 (362)	2057 (329)	2003 (278)	1604 (233)	1832 (138)
R-factor[d]	0.158 (0.190)	0.212 (0.316)	0.173 (0.212)	0.167 (0.226)	0.117 (0.210)
R-free	0.189 (0.192)	0.247 (0.340)	0.239 (0.250)	0.201 (0.239)	0.138 (0.225)

Table 1. Cont.

Phasing	Remote	Peak	Inflection point	Overall	
Number of atoms	3927	9799	10974	4006	1019
Average B/Wilson B (Å²)	18.4/13.9	49.5/55.1	32.1/25.1	19.1/16.5	22.1/15.6
Ramachandran statistics (%)	98.9/100.0	96.7/99.9	98.5/100.0	98.8/100.0	100.0/100.0
r.m.s.d. bonds (Å)/angles (˚)	0.012/1.5	0.016/1.3	0.014/1.4	0.013/1.5	0.013/1.6
PDB code	4D0U	4D1F	4D1G	4D0V	4UMI

[a]Figure of merit=cos(phase error).
[b]41.5% solvent content.
[c]Values in parentheses are for the highest resolution bin (where applicable).
[d]$R_{symm}=\Sigma_h\Sigma_i|I_{hi}-<I_h>|/\Sigma_h\Sigma_i|I_{hi}|$, where I_{hi} is the intensity of the ith measurement of the same reflection and $<I_h>$ is the mean observed intensity for that reflection.

doi:10.1371/journal.pone.0114373.t001

Results and Discussion

The structure of the SnAdV-1 fibre head domain was determined by multi-wavelength anomalous diffraction up to 1.6 Å resolution, using data collected from a selenomethionine derivative crystal as described [26]. Four monomers were present in the asymmetric unit, three (chains A, B and C) forming the biological trimer and the other (chain D) forming a trimer with two crystallographically equivalent monomers in the crystal (space group $I2_13$ has a three-fold crystallographic symmetry axis). Phasing statistics were very good (Table 1). Amino acids from the N-terminal T7 and 6xHis tags could not be modelled in the structure due to lack of density, as was also the case for residues 234–236 of each of the chains and residue Lys345 of chains A, B and C. Using NCS-restraints, the structures of both the seleno-methionine variant and native protein could be refined to low R-values at 1.6 and 1.7 Å resolution, respectively, with good geometry and Ramachandran statistics (Table 1). The head domain, with its eight-stranded beta-sandwich, starts at residue 238.

The structures of $P2_12_12_1$ crystal forms were solved by molecular replacement using a trimer of the determined structure as a template and refined using NCS-restraints at 2.7 and 1.9 Å resolution, respectively. The two different crystal forms belonging to the orthorhombic space group $P2_12_12_1$ both had four complete trimers in the asymmetric unit.

The purified 171–345 construct protein crystallized in space group $F23$ after a period of about one year. After structure solution by molecular replacement, it was noted that density for residues 171–231 was absent. The asymmetric unit of the crystals contains one monomer of the SnAdV1 fibre head, with all the residues of the fibre head (Pro232 to Lys345) being well-resolved. Coordinates and individual atom anisotropic temperature factors were refined at 1.33 Å resolution, leading to excellent agreement of the model with the data.

The fact that density for residues 171–231 was absent even when maps were calculated using low-resolution reflections only, combined with the long lag-time before crystallization, indicates a possible proteolysis event during crystallization. Two other observations support this hypothesis. The first is that there is no room in the crystal lattice at the bottom of the head domain to accommodate a shaft domain (S1 Figure); the second is that residues 232–234 point away from the three-fold trimer axis and away from each other, instead of downwards towards a potential shaft domain. The electron density for these residues is clear enough to make this interpretation reliable, while the low refinement R-factors suggests we are not missing a major part of the structure in our crystallographic model. Disorder predictions by the DISEMBL program [43] suggest that residues 230–236 have a higher probability of being disordered (S2 Figure), which also suggests the head-shaft junction of the fibre may be flexible and more accessible to proteases than the head domain.

When the structures of the fibre head monomer of the different crystal forms are superimposed, no significant differences in main chain conformations were observed. The r.m.s.d. (root mean square difference) between the structures is less than 0.38 Å and even the loop regions superimpose very well, suggesting little flexibility. When trimers are superimposed, the r.m.s.d. is less than 0.5 Å, suggesting the orientation of the monomers in the trimer is also fixed. Given the structural similarity between the crystal forms, the description below is based on the highest-resolution structures obtained, but is general to all structures.

The SnAdV-1 fibre head is the first Atadenovirus protein structure to be solved at atomic resolution (Fig. 1). The head domain starts at residue 238 and each monomer contains an eight-stranded beta-sandwich. Despite the low sequence identity with other fibre heads, the topology of the beta-sandwich is identical to that of known adenovirus fibre head structures and contains ABCJ and GHID beta-sheets (the E- and F-strands in the long DG-loop of human adenoviruses 5 and 2 [6,7] are absent). However, it is significantly more compact (Fig. 2C), making the 107-amino acid long SnAdV-1 fibre head the smallest adenoviral fibre head structure known. It has a diameter of 4.6 nm and a height of 3.8 nm (compared to a diameter of 6.2 nm and a height of 4.0 nm for the HAdV-5 fibre head [6]). The SnAdV-1 fibre head may be considered a "minimal" adenovirus fibre head fold, although smaller fibre trimerization domains are known, such as the bacteriophage T4 foldon [44–45].

In the trimer, the ABCJ-sheet is partially buried, facing the inside, while the GHID-sheet is mainly solvent-exposed. This means that the ABCJ-sheet contributes the majority of inter-monomer contacts. The strands making up the buried sheet are longer than those of the exposed sheet (average of ten residues per strand *vs.* six). The beta-strands in the structure are connected by either loops or beta-turns. Seven such connections exist; three loops (CD, DG and IJ) of variable size and four beta-turns (AB, BC, GH and HI) of two residues each. The CD and IJ loops contain 7 residues each, while the DG loop is longer, 16 residues. In SnAdV-1, an alpha-helix of eight residues is present in the DG-loop, rather than beta-strands like in Human Adenovirus 5.
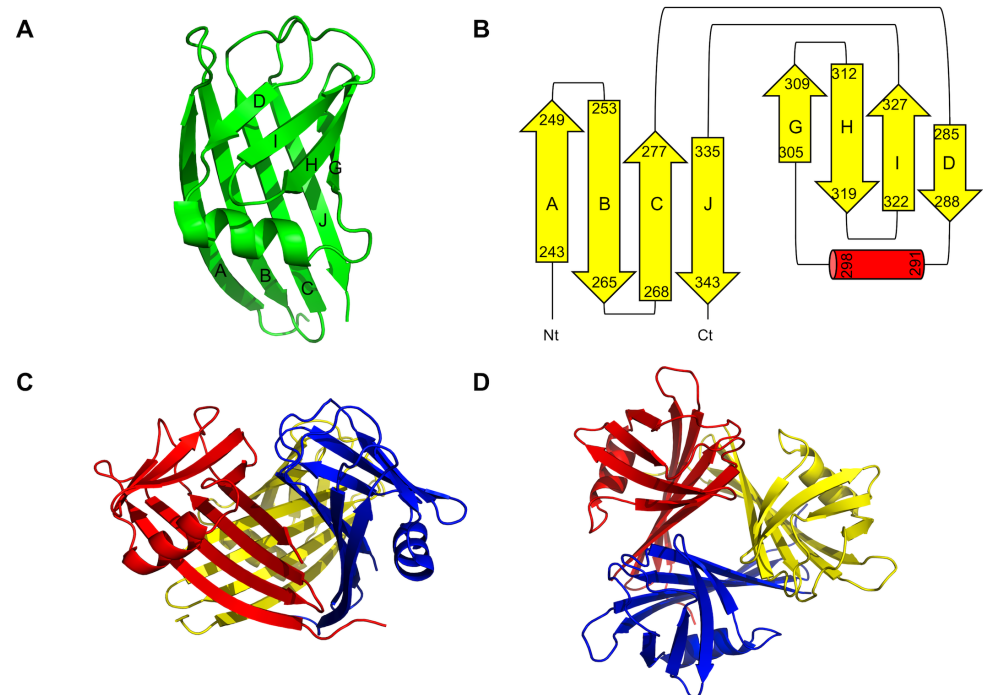
Figure 1. Structure of the Snake Atadenovirus 1 fibre head. A. Monomer structure. The beta-strands are labeled. B. Topology. The ABCJ and GHID beta-sheets are coloured yellow, the alpha-helix in the DG-loop is shown in red. C. Trimer structure, side view, with the three monomers coloured differently. D. Trimer structure, top view.
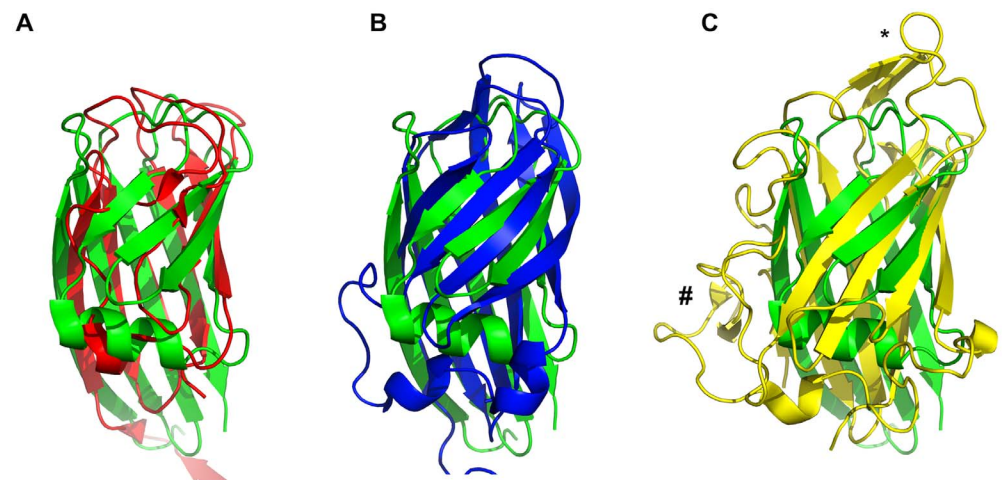
doi:10.1371/journal.pone.0114373.g001

Figure 2. Structural comparison with other viral receptor-binding proteins. Superposition of the SnAdV-1 fibre head monomer structure (green) onto the bacteriophage TP901-1 receptor-binding protein monomer (A; PDB entry 2F0C; red), onto the avian reovirus fibre head domain monomer (B; PDB entry 2BT7; blue) and the HAdV-37 fibre head monomer (C; PDB entry 2WBW; yellow). The SnAdV-1 fibre head monomer is in the same orientation as in Fig. 1A. The top of the trimer is indicated with * and the side with #.

doi:10.1371/journal.pone.0114373.g002

As mentioned, the fibre head of SnAdV-1 has little sequence identity with fibre heads of known structure. However, fibres from other adenoviruses, from reoviruses as well as receptor-binding proteins from bacteriophages were identified with a similar fold (Fig. 2). A DALI search [46] showed receptor binding protein of bacteriophages TP901-1 [47] and p2 [48] as the closest match with Z-values of around 7 (Fig. 2A). According to Holm et al. [46], significant similarities have a Dali Z-score above 2 and they usually correspond to similar folds. Strong matches have a Z-score above n/10−4, where n is the number of residues in the query structure, giving a Z-value cut-off of around 6 in this particular case. Further hits included the mammalian and avian reovirus attachment proteins sigma1 [49] and sigmaC [50, 51]. All these proteins share the same ABCJ-GHID beta-sandwich topology. An evolutionary relationship between adenovirus and reovirus fibres has been proposed before, based on structural similarity between their triple beta-spiral repeat shaft and beta-structured head domains [5, 49]. Strengthening this idea, the SnAdV-1 fibre head has close similarity, more than any other adenovirus heads, to reovirus attachment proteins sigma1 and sigmaC. However, sigma1 and sigmaC have a circular arrangement of the beta-structured head domain, a "beta-barrel", with strands C and H carrying kinks, whereas SnAdV-1 fibre head has a sandwich like appearance with no observable kinks in any of its strands (Fig. 2B).

Spinelli *et al.* proposed an evolutionary relationship between phage receptor-binding domains and adenovirus and reovirus fibre head domains [48]. The small (just under 100 residues per monomer), trimeric, C-terminal receptor binding domains of TP901-1 and p2 bacteriophages are beta-barrels made up of six and seven anti-parallel beta-strands, respectively. Their compact structures are comparable to the SnAdV-1 fibre head in dimensions and secondary structure, despite having fewer beta-strands (Fig. 2A).

Among adenovirus fibre head domains, SnAdV-1 fibre head is most similar to the fibre heads of Porcine Adenovirus 4 [52] and Human Adenoviruses 19p and 37 [53]. All of these structures have a similar beta-sandwich arrangement, containing ABCJ- and GHID-sheets, but unlike the SnAdV-1 fibre head, structures HAdV-19p and HAdV-37 have longer loops connecting the beta-strands. Human Adenovirus 19p and 37 fibre head bind both the Coxsackievirus and Adenovirus Receptor protein (CAR) and/or sialic acid [19]. However, in the SnAdV-1 fibre head domain, the loops that interact with CAR (on the side of the trimer) or sialic acid (on the top of the trimer) are significantly shorter and have different conformations (Fig. 2C). Also, unlike fibre heads of HAdV-37 and HAdV-19p, which have a high predicted pI, the predicted pI of SnAdV-1 fibre head is around 5.

The trimeric packing of SnAdV-1 fibre head is highly stable, exemplified by the fact that to visualize monomers on a sodium dodecylsulphate-gel, boiling the protein in protein sample buffer containing dodecylsulphate for a few minutes is necessary before sample loading [26]. This is also true for other virus and phage fibre proteins [54]. Each monomer has a total solvent accessible surface area of 5.9×10^3 Å^2, out of which 1.4×10^3 Å^2 (24%) gets buried upon trimer formation.

Eleven hydrogen bonds and ten salt bridges are contributed by each monomer to the assembly. The majority of these residues responsible for inter-monomer interactions are located on strands B, C and J. Approximately 8.5 kcal/mol of energy is required to dissociate the trimer into monomers, as calculated by PISA [55].

Although surface-exposed loops play the most important roles in adenovirus fibre-receptor interaction, surface charge may also have an effect [9, 53]. Positively charged patches are naturally inclined to bind negatively charged molecules such as sialic acid, which is a common terminal glycan on cell surface proteins. The surface of the SnAdV-1 fibre head is mixed in its predicted charge distribution and extensive positive patches are absent (Fig. 3). There is an extended negatively charged patch on the side of the trimer, however, no known positively-charged adenovirus receptors have been described. Most of the specific residues that bind the known human adenovirus receptors CD46 [56] or desmoglein-2 [57] are absent in the SnAdV-1 fibre head. Based on the HAdV-11 co-crystal structure with CD46 [56], Arg279, Arg280, Asp284 and Gln305 are the most important residues for interaction. Of these, only Asp284 may be conserved in the SnAdV-1 fibre head (Asp319). Furthermore, the DG- and HI-loops are in a very different orientation. Amino acids which have been shown to be important for desmoglein-2 binding with HAdV-3 and HAdV-14 [57] are also not conserved in the SnAdV-1 fibre head. Finally, the SnAdV-1 fibre head domain does not contain putative heparan sulphate binding sequences [58], although a KKIK sequence at the very amino-terminus (residues 2–5) of the fibre could play this role.

Extensive surface loops present on fibre heads of other adenoviruses may favour the possibility of altering the antigenic nature of the fibre head by mutation; the relative absence of loops suggests that SnAdV-1 and perhaps Atadenoviruses in general have less need for this mechanism. Knowledge of the snake immune system is limited, although, like in mammals, it consists of innate, cell-mediated and humoral mechanisms [59]. Since reptiles are ectotherm organisms, their immune system is highly sensitive to temperature or seasonal changes. Perhaps viruses like SnAdV-1 can profit from less favourable conditions to avoid interactions with components of the immune system.

In conclusion, the fibre head domain of Snake Adenovirus 1 is the first Atadenovirus protein for which the atomic structure has been solved. The compact trimeric structure is very stable as a result of extensive non-covalent interactions between its monomeric units, forming the trimer. The structure is the smallest among known adenovirus fibre head structures, while it retains the same overall beta-sandwich topology and may therefore be seen as a "minimal" adenovirus fibre head fold. The structure is even more similar to the head domains of certain dsDNA bacteriophage receptor binding proteins and the dsRNA-virus (reovirus) fibres, which prompts the question whether this similarity is the result of divergent or convergent evolution, or perhaps horizontal gene transfer events.

An important application of adenoviruses is their use as vectors for human gene and cancer therapy and for vaccination purposes. Animal adenoviruses may be of
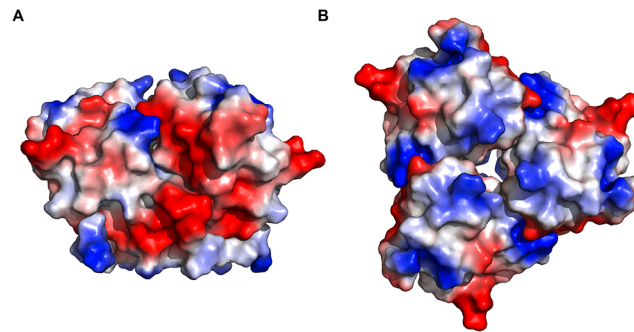
Figure 3. Qualitative electrostatic surface diagram of the SnAdV-1 fibre head. A. Side view in the same orientation as Fig. 1C. B. Top view in the same orientation as Fig. 1D.

doi:10.1371/journal.pone.0114373.g003

special interest due to the lack of neutralizing antibodies in human sera against them. The detailed structure of the SnAdV-1 fibre head and other animal adenovirus fibre heads, together with future identification of their natural receptors, may lead to the development of new strategies to target adenovirus vectors to cells of interest.

Supporting Information

S1 Figure. Packing of the *F*23 space group crystal. A. Bottom view. One SnAdV-1 fibre head trimer is shown in cyan, orange and blue. Asterisks indicate the amino-terminal Glu232, while a hash sign indicates where the shaft domain is expected to be. B. Side view of A. There is not enough room for a shaft domain in the crystal packing; furthermore, the amino-terminal ends of the structure point away from each other and from the three-fold symmetry axis where the shaft domain is expected to be.
doi:10.1371/journal.pone.0114373.s001 (TIFF)

S2 Figure. Disorder prediction (DISEMBL program). A peak in predicted disorder probability between residues 230 and 236 suggests there may be some flexibility between the putative shaft domain and the head domain.
doi:10.1371/journal.pone.0114373.s002 (TIFF)

Acknowledgments

Author Contributions

References

1. **Philipson L** (1995) Adenovirus - an eternal archetype. Curr Top Microbiol 199: 1–24.

2. **San Martín C** (2012) Latest insights on adenovirus structure and assembly. Viruses 4: 847–877.

3. **Rux JJ, Burnett RM** (2000) Type-specific epitope locations revealed by X-ray crystallographic study of adenovirus type 5 hexon. Molecular Therapy 1: 18–30.

4. **Zubieta C, Schoehn G, Chroboczek J, Cusack S** (2005) The structure of the human adenovirus 2 penton. Mol Cell 17: 121–135.

5. **van Raaij MJ, Mitraki A, Lavigne G, Cusack S** (1999) A triple beta-spiral in the adenovirus fibre shaft reveals a new structural motif for a fibrous protein. Nature 401: 935–938.

6. **Xia D, Henry LJ, Gerard RD, Deisenhofer J** (1994) Crystal structure of the receptor-binding domain of adenovirus type 5 fibre protein at 1.7 Å resolution. Structure 2: 1259–1270.

7. **van Raaij MJ, Louis N, Chroboczek J, Cusack S** (1999) Structure of the human adenovirus serotype 2 fiber head domain at 1.5 Å resolution. Virology 262: 333–343.

8. **Bergelson JM, Cunningham JA, Droguett G, Kurt-Jones EA, Krithivas A, et al.** (1997) Isolation of a common receptor for Coxsackie B viruses and adenoviruses 2 and 5. Science 275: 1320–1323.

9. **Bewley MC, Springer K, Zhang YB, Freimuth P, Flanagan JM** (1999) Structural analysis of the mechanism of adenovirus binding to its human cellular receptor, CAR. Science 286: 1579–1583.

10. **van Raaij MJ, Chouin E, van der Zandt H, Bergelson JM, Cusack S** (2000) Dimeric structure of the coxsackievirus and adenovirus receptor D1 domain at 1.7 A resolution. Structure 8: 1147–1155.

11. **Arnberg N, Kidd AH, Edlund K, Olfat F, Wadell G** (2000) Initial interactions of subgenus D adenoviruses with A549 cellular receptors: sialic acid versus alpha(v) integrins. J Virol 74: 7691–7693.

12. **Segerman A, Atkinson JP, Marttila M, Dennerquist V, Wadell G, et al.** (2003) Adenovirus type 11 uses CD46 as a cellular receptor. J Virol 77, 9183–9191.

13. **Short JJ, Vasu C, Holterman MJ, Curiel DT, Pereboev A** (2006) Members of adenovirus species B utilize CD80 and CD86 as cellular attachment receptors. Virus Res 122: 144–153.

14. **Wang H, Li ZY, Liu Y, Persson J, Beyer I, et al.** (2011) Desmoglein 2 is a receptor for adenovirus serotypes 3, 7, 11 and 14. Nature Med 17: 96–104.

15. **Wickham TJ, Mathias P, Cheresh DA, Nemerow GR** (1993) Integrins alpha v beta 3 and alpha v beta 5 promote adenovirus internalization but not virus attachment. Cell 73: 309–319.

16. **Hess M, Cuzange A, Ruigrok RW, Chroboczek J, Jacrot B** (1995) The avian adenovirus penton: two fibres and one base. J Mol Biol 252: 379–385.

17. **Harrach B, Benko M, Both GW, Brown M, Davison AJ, et al.** (2011) Family *Adenoviridae*. In: King AMQ, Adams MJ, Carstens EB, Lefkowitz EJ, editors, Virus Taxonomy: Classification and Nomenclature of Viruses. Ninth Report of the International Committee on Taxonomy of Viruses. San Diego: Elsevier, 95–111.

18. **Seiradake E, Lortat-Jacob H, Billet O, Kremer EJ, Cusack S** (2006) Structural and mutational analysis of human Ad37 and canine adenovirus 2 fiber heads in complex with the D1 domain of coxsackie and adenovirus receptor. J Biol Chem 281: 33704–33716.

19. **Seiradake E, Henaff D, Wodrich H, Billet O, Perreau M, et al.** (2009) The cell adhesion molecule CAR and sialic acid on human erythrocytes influence adenovirus *in vivo* biodistribution. Plos Pathog 5: 00277.

20. **Guardado-Calvo P, Llamas-Saiz AL, Fox GC, Langlois P, van Raaij MJ** (2007) Structure of the C-terminal head domain of the fowl adenovirus type 1 long fiber. J Gen Virol 88: 2407–2416.

21. **El Bakkouri M, Seiradake E, Cusack S, Ruigrok RW, Schoehn G** (2008) Structure of the C-terminal head domain of the fowl adenovirus type 1 short fibre. Virology 378: 169–176.

22. **McConnell MJ, Imperiale MJ** (2004) Biology of adenovirus and its use as a vector for gene therapy. Hum Gene Ther 15: 1022–1033.

23. **Bachtarzi H, Stevenson M, Fisher K** (2008) Cancer gene therapy with targeted adenoviruses. Expert Opin Drug Del 5: 1231–1240.

24. **Löser P, Cichon G, Jennings G, Both G, Hofmann C** (1999) Ovine adenovirus vectors promote efficient gene delivery in vivo. Gene Ther Mol Biol 4: 33–43.

25. **Pénzes JJ, Menéndez-Conejero R, Condezo GN, Ball I, Papp T, et al.** (2014) Molecular characterization of a lizard adenovirus reveals the first Atadenovirus with two fiber genes and the first adenovirus with either one short or three long fibers per penton. J Virol 88: 11304–11314.

26. **Singh AK, Menéndez-Conejero R, San Martín C, van Raaij MJ** (2013) Crystallization of the C-terminal domain of the fibre protein from snake adenovirus 1, an atadenovirus. Acta Cryst F 69: 1374–1379.

27. **Singh AK, Ballmann MZ, Benkő M, Harrach B, van Raaij MJ** (2013) Crystallization of the C-terminal head domain of the fibre protein from a siadenovirus, turkey adenovirus 3. Acta Cryst F 69: 1135–1139.

28. **Juhasz A, Ahne W** (1993) Physicochemical properties and cytopathogenicity of an adenovirus-like agent isolated from corn snake (Elaphe guttata). Arch Virol 130: 429–439.

29. **Farkas SL, Harrach B, Benko M** (2008) Completion of the genome analysis of snake adenovirus type 1, a representative of the reptilian lineage within the novel genus Atadenovirus. Virus Res 132: 132–139.

30. **Myers E, Miller W** (1988) Optimal Alignments in Linear Space. Comput Appl Biosc 4: 11–17.

31. **Pantelic RS, Lockett LJ, Rothnagel R, Hankamer B, Both GW** (2008) Cryoelectron microscopy map of Atadenovirus reveals cross-genus structural differences from human adenovirus. J Virol 82: 7346–7356.

32. **Vonrhein C, Blanc E, Roversi P, Bricogne G** (2007) Automated structure solution with autoSHARP. Meth Mol Biol 364: 215–230.

33. **Sheldrick GM** (2010) Experimental phasing with SHELXC/D/E: combining chain tracing with density modification. Acta Cryst D 66: 479–485.

34. **Abrahams JP, Leslie AG** (1996) Methods used in the structure determination of bovine mitochondrial F1 ATPase. Acta Cryst D 52: 30–42.

35. **Langer G, Cohen SX, Lamzin VS, Perrakis A** (2008) Automated macromolecular model building for X-ray crystallography using ARP/wARP version 7. Nat Protoc 3: 1171–1179.

36. **Emsley P, Lohkamp B, Scott WG, Cowtan K** (2010) Features and development of Coot. Acta Cryst D 66: 486–501.

37. **Murshudov GN, Skubak P, Lebedev AA, Pannu NS, Steiner RA, et al.** (2011) REFMAC5 for the refinement of macromolecular crystal structures. Acta Cryst D 67: 355–367.

38. **Brünger AT** (1992) Free R value: a novel statistical quantity for assessing the accuracy of crystal structures. Nature 355: 472–475.

39. **Winn MD, Ballard CC, Cowtan KD, Dodson EJ, Emsley P, et al.** (2011) Overview of the CCP4 suite and current developments. Acta Cryst D 67: 235–242.

40. **McCoy AJ, Grosse-Kunstleve RW, Adams PD, Winn MD, Storoni LC, et al.** (2007) Phaser crystallographic software. J Appl Cryst 40: 658–674.

41. **Chen VB, Arendall WB, Headd JJ, Keedy DA, Immormino RM, et al.** (2010). MolProbity: all-atom structure validation for macromolecular crystallography. Acta Cryst D 66: 12–21.

42. **McNicholas S, Potterton E, Wilson KS, Noble ME** (2011) Presenting your structures: the CCP4mg molecular-graphics software. Acta Cryst D 67: 386–394.

43. **Linding R, Jensen LJ, Diella F, Bork P, Gibson TJ, et al.** (2003) Protein disorder prediction: implications for structural proteomics. Structure 11: 1453–1459.

44. **Tao Y, Strelkov SV, Mesyanzhinov VV, Rossmann MG** (1997) Structure of bacteriophage T4 fibritin: a segmented coiled coil and the role of the C-terminal domain. Structure 5: 789–798.

45. **Papanikolopoulou K, Teixeira S, Belrhali H, Forsyth VT, Mitraki A, et al.** (2004) Adenovirus fibre shaft sequences fold into the native triple beta-spiral fold when N-terminally fused to the bacteriophage T4 fibritin foldon trimerisation motif. J Mol Biol 342: 219–227.

46. **Holm L, Rosenstrom P** (2010) Dali server: conservation mapping in 3D. Nucl Acids Res 38: W545–549.

47. **Spinelli S, Campanacci V, Blangy S, Moineau S, Tegoni M, et al.** (2006) Modular structure of the receptor binding proteins of Lactococcus lactis phages. The RBP structure of the temperate phage TP901-1. J Biol Chem 281: 14256–14262.

48. **Spinelli S, Desmyter A, Verrips CT, Dehaard HJ, Moineau S, et al.** (2006) Lactococcal bacteriophage p2 receptor-binding protein structure suggests a common ancestor gene with bacterial and mammalian viruses. Nat Struct Mol Biol 13: 85–89.

49. **Chappell JD, Prota AE, Dermody TS, Stehle T** (2002) Crystal structure of reovirus attachment protein sigma1 reveals evolutionary relationship to adenovirus fibre. EMBO J 21: 1–11.

50. **Guardado Calvo P, Fox GC, Hermo Parrado XL, Llamas-Saiz AL, Costas C, et al.** (2005) Structure of the carboxy-terminal receptor-binding domain of avian reovirus fibre sigmaC. J Mol Biol 354: 137–149.

51. **Guardado-Calvo P, Fox GC, Llamas-Saiz AL, van Raaij MJ** (2009) Crystallographic structure of the alpha-helical triple coiled-coil domain of avian reovirus S1133 fibre. J Gen Virol 90: 672–677.

52. **Guardado-Calvo P, Muñoz EM, Llamas-Saiz AL, Fox GC, Kahn R, et al.** (2010) Crystallographic structure of porcine adenovirus type 4 fibre head and galectin domains. J Virol 84: 10558–10568.

53. **Burmeister WP, Guilligay D, Cusack S, Wadell G, Arnberg N** (2004) Crystal structure of species D adenovirus fiber knobs and their sialic acid binding sites. J Virol 78: 7727–7736.

54. **Mitraki A, Papanikolopoulou K, van Raaij MJ** (2006) Natural triple beta-stranded fibrous folds. Adv Protein Chem 73: 97–124.

55. **Krissinel E, Henrick K** (2007) Inference of macromolecular assemblies from crystalline state. J Mol Biol 372: 774–797.

56. **Persson BD, Reiter DM, Marttila M, Mei YF, Casasnovas JM, et al.** (2007) Adenovirus type 11 binding alters the conformation of its receptor CD46. Nat Struct Mol Biol 14: 164–166.

57. **Wang H, Yumul R, Cao H, Ran L, Fan X, et al.** (2013) Structural and functional studies on the interaction of adenovirus fiber knobs and desmoglein 2. J Virol 87: 11346–11362.

58. **Dechecchi MC, Tamanini A, Bonizzato A, Cabrini G** (2000) Heparan sulfate glycosaminoglycans are involved in adenovirus type 5 and 2-host cell interactions. Virology 268: 382–390.

59. **Zimmerman LM, Vogel LA, Bowden RM** (2010) Understanding the vertebrate immune system: insights from the reptilian perspective. J Exp Biol 213: 661–671.